THE JOURNAL OF PHYSICAL CHEMISTRY LETTERS
A JOURNAL OF THE AMERICAN CHEMICAL SOCIETY

pubs.acs.org/JPCL
Letter

The Properties That Allow Tuning the Reduction Potentials over a Volt Range in Biological Iron/Sulfur Clusters

Busra Dereli, Marcel D. Baer, John W. Peters,* and Simone Raugei*

Cite This: J. Phys. Chem. Lett. 2025, 16, 4602−4606
Read Online

ABSTRACT: [4Fe-4S] clusters are ubiquitous in biology and are crucial to the more salient processes in energy metabolism, serving as intermediates in inter- and intramolecular electron transfer pathways. The [4Fe-4S] clusters are more prevalent, serving a variety of functions, and can remarkably adopt a surprising range of reduction potentials spanning more than 1 V. The characteristics of the environment, including charge, solvent access, and geometric distortion, finely modulate the reduction potential of iron/sulfur clusters. However, prior research has not yet systematically addressed cause and effect. In this work, we conducted a thorough theoretical assessment of how charge distribution and structural distortion contribute to the full range of reductions exhibited by biological [4Fe-4S] clusters. The work shows that the most significant contributions can be predicted for electrostatic interactions, which are directionally biased.

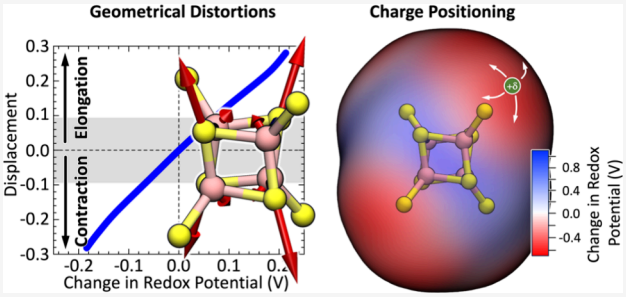

Cubes composed of four iron ions (Fe^{2+} and Fe^{3+}) and four sulfide ions (S^{2-}), commonly referred to as [4Fe-4S] clusters, are present in all life forms, where they play a direct role in catalysis or electron trafficking in metabolism.[1−3] For the large family of radical S-adenosylmethionine (SAM)-dependent enzymes, a single [4Fe-4S] cluster is bound in a site-specific manner, with three Fe ions coordinated by three cysteine residues, leaving one Fe site available for binding SAM.[4,5] In electron trafficking, the Fe ions of [4Fe-4S] clusters are typically bound to proteins by four cysteine residues in small (∼6 kDa) electron carriers known as ferredoxins or as part of various redox cofactor-containing complexes, such as the respiratory complexes of the electron transport chain or in photosynthetic reactions centers.[6,7] The most common Fe oxidation states of these clusters are $2Fe^{2+}$ and $2Fe^{3+}$ or $3Fe^{2+}$ and $1Fe^{3+}$, referred to as $[4Fe\text{-}4S]^{2+}$ and $[4Fe\text{-}4S]^{1+}$, respectively. This reflects the summation of four Fe oxidation states and four S^{2-}.[6,8] Electrons are delocalized differently within the $[4Fe\text{-}4S]^{2+}$ and $[4Fe\text{-}4S]^{1+}$ clusters. In the case of $[4Fe\text{-}4S]^{2+}$, delocalization produces two equivalent rhombohedral halves, while in the $[4Fe\text{-}4S]^{1+}$ cluster, it encompasses the entire cubane.[9]

Coordinated by four cysteines, these simple [4Fe-4S] clusters are highly conserved in structure.[10−12] The most significant differences stem from the constraints on the cluster due to protein coordination and the protein electric field in which they are embedded. Surprisingly, despite this apparent high level of conservation, the [4Fe-4S] clusters show a variety of reduction potentials that range up to 1 V.[13] Therefore, the subtleties of protein coordination and the surrounding environment presumably have a significant impact on the variability of these reduction potentials.[14−16] Given the differences in charge and electron delocalization of the $[4Fe\text{-}4S]^{2+}$ and $[4Fe\text{-}4S]^{1+}$ clusters, it is intuitive that the charge or dielectric properties of the protein environment[12,17] and the coordination-mediated geometric distortions of the clusters[18] should influence the reduction potentials.[19,20] However, it is challenging to envision how these factors contribute to the broad observed potential range. Traditionally, accurately estimating reduction potentials based on the protein environment has been difficult[21−24] despite many recent efforts.

We aimed to use an alternative approach to clarify the influence of the protein environment on tuning the reduction potentials of [4Fe-4S] clusters. We concentrated on the reduction potential that describes the biologically relevant interconversion between the $[4Fe\text{-}4S]^{2+}$ and $[4Fe\text{-}4S]^{1+}$ states. We applied various geometric distortions, charge magnitudes, and charge positions to identify the key contributors and assess the extent of differences that may be implicated.

We conducted density functional theory (DFT) calculations using the broken symmetry framework[9,25] on a simplified model of cysteine-ligated [4Fe-4S] clusters[24,26] (Figure 1), in which cysteine thiolate ligands were represented as methyl thiols. The initial model possesses D_{2d} symmetry, characterized

Received: February 27, 2025
Revised: April 7, 2025
Accepted: April 10, 2025
Published: May 1, 2025

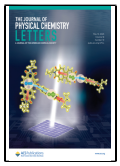

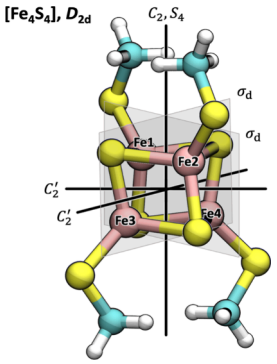

Figure 1. Structure of methylthiolate coordinated [4Fe-4S] cluster. The symmetry operations of the groups for the point group D_{2d} are highlighted and chemical groups are colored with hydrogens in shaded white, carbons in cyan, sulfurs in yellow, and irons in rust.

by a principal C_2 axis and S_4 axes and two perpendicular C'_2 axes.[27] We monitored the change in gas-phase vertical electron affinity (VEA) as a proxy for the change in redox potential, $E^\circ \approx E_{VEA}$, induced by structural and electrostatic perturbations (see Supporting Information for details).

The arrangement depicted in Figure 1 resembles the two sets of cysteine pincers found in the [4Fe-4S] clusters of ferredoxins, which are connected by a 2-fold screw axis or rotation of 180°. There are subtle differences in electron delocalization within the molecular orbital configurations of [4Fe-4S] clusters in the $[4Fe\text{-}4S]^{2+}$ and $[4Fe\text{-}4S]^{+}$ oxidation states. Certain geometric distortions of the clusters could affect the orbital configurations,[28,29] stabilizing one oxidation state versus the other, thereby influencing the cluster reduction potential.

Embedded within the framework of geometric distortions is the symmetry reduction that occurs when a perfect cubane is distorted.[30] This can be treated systematically through computation. Minimizing the methyl thiol-coordinated [4Fe-4S] cluster results in a slightly anisotropic distorted structure characterized by eight short and four long Fe−S distances,[31,14] respectively, nearly perpendicular and parallel to the C_2 axis (Figure 1). The decomposition of the motion of the [4Fe-4S] cluster into normal modes and molecular symmetry analyses indicate that any distortions invariant for the totally symmetric representation of the subgroup C_{2v} of D_{2d} have the most significant effect on the redox potential (modes A_1 and B_2, Figure 2a). These distortions preserve the principal axis C_2 and the reflection planes σ_d (see Supporting Information). An example of such motion is the top mode A_1, which is localized on the cubane. As shown in Figure 2b, a slight change in geometry along this mode leads to significant variations in redox potential. Distortions along the A_1 and B_2 modes primarily stabilize or destabilize the frontier orbitals. (Figure 2c). These orbitals are mainly localized on the Fe atoms and primarily originate from the *d* orbitals of the metal ions.

We can apply the normal mode decomposition to investigate the effects of dilations along the C_2 axis and the pseudo-C_3 identified by the Fe atoms and their opposing inorganic S atoms, two distortions observed in synthetic models.[14,27] These distortions are mostly a linear combination of the top two A_1 and B_2 modes. Consequently, our model forecasts a significant impact on the redox potential. For instance, consistent with experimental reports, compression along the C_2 long axis[28] results in changes to more reducing or negative

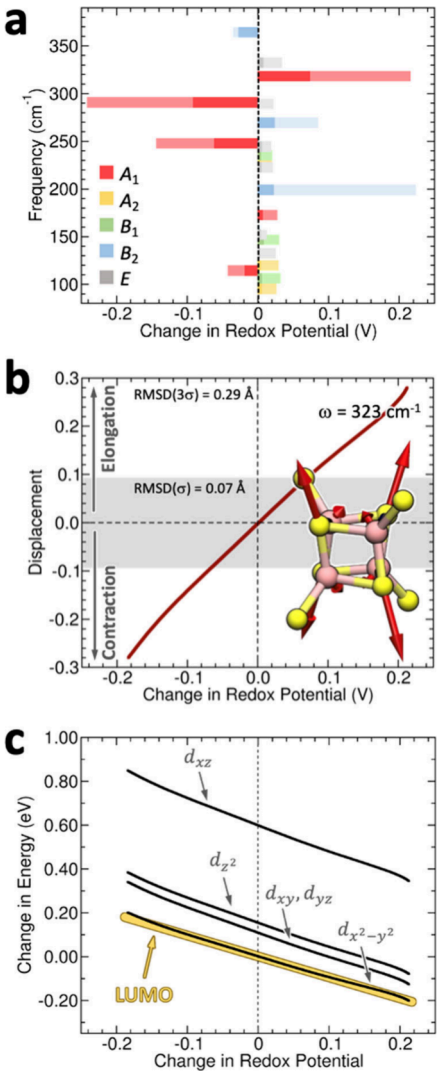

Figure 2. Effect of structural distortions on the redox potential of $(Fe_4S_4)(SCH_3)_4$. **Panel a:** Change in redox potential for atomic displacements up to $+3\sigma$ along a given normal mode of vibration, where σ is the root-mean-square deviation of a harmonic oscillator at 298 K. The dark color shades demark $+1\sigma$ displacements. The normal modes are labeled according to their symmetry. **Panel b:** Change in redox potential for displacements along the top A_1 mode. The shaded area indicates displacements between $\pm\sigma$, while the full range corresponds to displacements between $\pm3\sigma$. The root-mean-square deviation of the atomic displacements at 1σ and 3σ are also reported. **Panel c:** Correlation between the change in redox potential and the energy of the Fe's d orbitals caused by the displacements in panel b.

potentials in a shallow curve.[19] In contrast, elongation along the same axis results in changes to more oxidizing or positive potentials in a much steeper manner (see Supporting Information). The magnitude of these differences is substantial and corresponds with the observed variations in the geometries of various ligated [4Fe-4S] cluster model complexes. One would expect a range greater than 100 mV. While the changes in reduction potential introduced by geometric distortions seem significant, they do not explain the differences seen in [4Fe-4S] clusters in natural and synthetic systems, where the range surpasses 1 V.[29]

We then assessed the electrostatic continuum and the influence of point charges near the cluster. A proximal charge is expected to affect the stabilization or destabilization of

https://doi.org/10.1021/acs.jpclett.5c00616
J. Phys. Chem. Lett. 2025, 16, 4602−4606

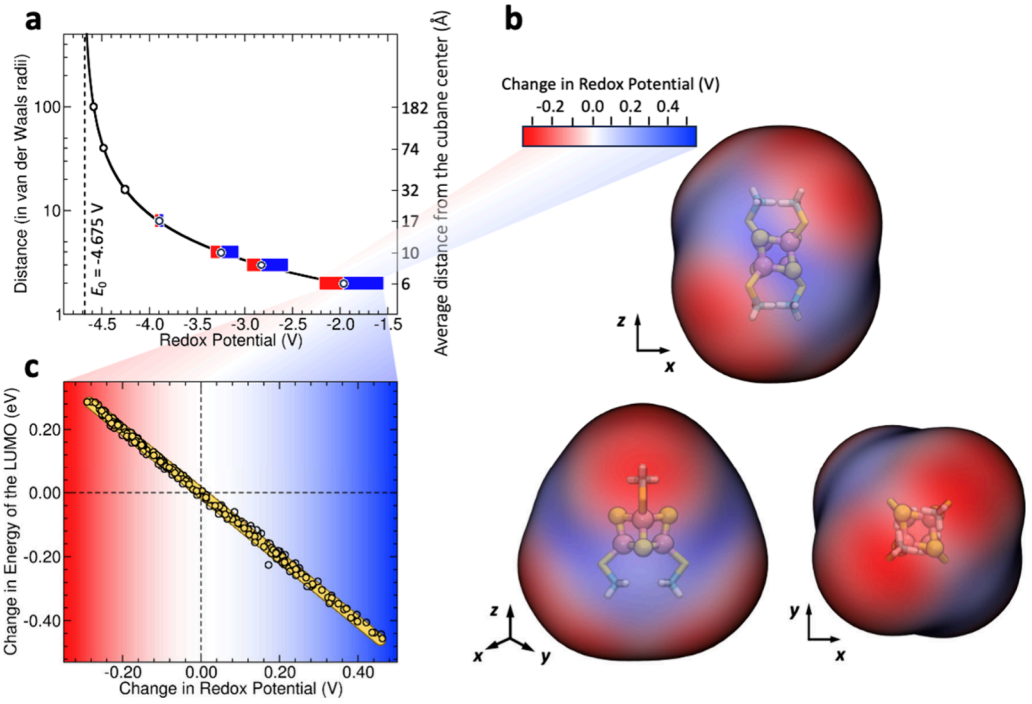

Figure 3. Effect of a positioned unitary positive charge on the reduction potential. **Panel a:** Dependence of the average and spread of the redox potential values as a function of the distance of the probe charge q = +1*e* from the van der Waals (vdW) surface of the cluster expressed in terms of vdW radii. The horizontal bars indicate the range of values of the redox potential rolling the probe charge on vdW isosurfaces, where red and blue indicate a negative and positive change from the average redox potential (circles). A vertical dashed line shows the limiting value of the redox potential (E_0) when the charge is at an infinite distance. For each vdW surface, the average distance from the cluster's center is also provided. **Panel b:** Change in redox potential from the average by positioning the probe charge at different locations on the vdW = 2 isosurface. **Panel c:** Correlation between redox potential and energy of the LUMO of the oxidized cluster for vdW = 2.

different oxidation states significantly.[32−34] For instance, a positive charge is expected to stabilize reduced states and favor more positive potentials.[11] Similarly, a nearby negative charge is expected to stabilize the oxidized state compared to the reduced state and promote more negative potentials. Introducing a point charge significantly influences the reduction potential, as expected. The extent of the shift depends greatly on both the magnitude and location of the charge. The data presented in Figures 3a and 3b demonstrate that at short distances, variations in the location of the charge lead to significant changes in the redox potential (Figure 3b). Beyond approximately 17 Å from the center of the cluster, the positioning of the charge becomes irrelevant (Figure 3a) as the field exerted by the charge becomes uniform within the cluster region. The anisotropy of the field generated by the charge at short distances introduces a strong positional dependence. A positive charge causes the most significant negative shift when it is located near the individual S^{2-} of the [4Fe-4S] cluster and the most positive shift when the charge is outside the van der Waals space of one of the coordinating cysteines. For charges positioned at a distance twice the van der Waals distance from the cluster, varying locations of the charge alter the redox potential by nearly 1 V per unit charge (Figure 3b). These results reflect the stabilization of the reduced state and an increase in the ease of cluster reduction by stabilizing the LUMO of the oxidized state and the HOMO of the reduced state (Figure 3c). The introduction of a negative charge mirrors the shift in the opposite direction. The perturbation caused by the point charge varies linearly with the magnitude of the charge, featuring an expected $1/\varepsilon$ screening effect due to the polarizable dielectric between the charge and complex.

In summary, we have conducted a thorough computational and theoretical assessment of the impact of geometrical distortions and point charges positioning as factors influencing the complete range of reductions associated with [4Fe-4S] clusters. The results indicate that geometric distortions within the limits of rational chemical bonding constraints offer important but limited control over reduction potentials. In contrast, electrostatic interactions in simulations across the full dielectric spectrum from gas to liquid water replicate the range observed experimentally for materials derived from biological systems. These effects were examined with greater detail by introducing a point change on van der Waals surfaces of increasing size. This analysis revealed that anisotropic electrostatic effects are most pronounced when the charge is closest to the cubane sulfides compared to the cysteinyl thiolates and that there is a linear relationship between charge magnitude and ionization potential. The observed range of ionization potentials was accompanied by notable differences in the coupling constants of Fe, indicating the overall tuning of reduction potentials caused by the offsetting charge of sulfides through these electrostatic interactions. The ability to model how charge and geometric distortion influence the tuning of reduction potentials in [4Fe-4S] clusters opens possibilities for treating computational reduction potential estimations in a formulaic manner. These findings can be conceptually applied to other redox cofactors. The results have broad implications for understanding the key features that govern the electronic properties and oxidation−reduction reactions of [4Fe-4S] clusters. These are the most ubiquitous and abundant examples of inorganic electron-transferring prosthetic groups essential to energy metabolism in all life forms.

https://doi.org/10.1021/acs.jpclett.5c00616
J. Phys. Chem. Lett. 2025, 16, 4602−4606

■ ASSOCIATED CONTENT

Supporting Information

The Supporting Information is available free of charge at https://pubs.acs.org/doi/10.1021/acs.jpclett.5c00616.

Details of the density functional theory calculations, decomposition of the cluster motion in normal modes, and evaluation of electrostatic effects and an extended discussion of the impact of geometric distortion and electrostatic fields (PDF)

Transparent Peer Review report available (PDF)

■ AUTHOR INFORMATION

Corresponding Authors

John W. Peters − *Physical Sciences Division, Pacific Northwest National Laboratory, Richland, Washington 99352, United States; Department of Chemistry and Biochemistry, University of Oklahoma, Norman, Oklahoma 73019, United States;* orcid.org/0000-0001-9117-9568; Email: jw.peters@ou.edu

Simone Raugei − *Physical Sciences Division, Pacific Northwest National Laboratory, Richland, Washington 99352, United States;* orcid.org/0000-0001-9118-8480; Email: simone.raugei@pnnl.gov

Authors

Busra Dereli − *Physical Sciences Division, Pacific Northwest National Laboratory, Richland, Washington 99352, United States*

Marcel D. Baer − *Physical Sciences Division, Pacific Northwest National Laboratory, Richland, Washington 99352, United States;* orcid.org/0000-0001-5223-0447

Complete contact information is available at: https://pubs.acs.org/10.1021/acs.jpclett.5c00616

Notes

The authors declare no competing financial interest.

■ ACKNOWLEDGMENTS

Funding was provided by the U.S. Department of Energy (DOE), Office of Science, Basic Energy Sciences (BES), Materials Sciences and Engineering Division, Biomolecular Materials Program, under FWP77876 (B.D. and M.D.B. for the normal mode analysis), the U.S. DOE/BES Chemical Sciences, Geosciences, and Biosciences Division, Physical Biosciences Program, under FWP 66476 (B.D., M.D.B., and S.R. for the electrostatic analysis), and the National Institutes of Health under grant 1R01GM1385920 (J.W.P. and S.R.). Computational resources were provided by the Molecular Sciences Computing Facility (MScF) in the environmental Molecular Sciences Laboratory, a U.S. Department of Energy (DOE) User Facility located at the Pacific Northwest National Laboratory (PNNL), and the National Energy Research Scientific Computing Center, supported by the Office of Science of the U.S. DOE. This work is authored by the Pacific Northwest National Laboratory operated by Battelle for the DOE under Contract number DE-AC05-76RL01830. The views expressed in the article do not necessarily represent the views of the DOE or the U.S. Government. The U.S. Government retains, and the publisher, by accepting the article for publication, acknowledges that the U.S. Government retains a nonexclusive, paid-up, irrevocable, worldwide license to publish or reproduce the published form of this work or allow others to do so for the U.S. Government purposes.

■ REFERENCES

(1) Beinert, H.; Holm, R. H.; Münck, E. Iron-Sulfur Clusters: Nature's Modular, Multipurpose Structures. *Science* **1997**, *277*, 653−659.

(2) Beinert, H. Iron-sulfur proteins: ancient structures, still full of surprises. *JBIC Journal of Biological Inorganic Chemistry* **2000**, *5*, 2−15.

(3) Noodleman, L. Fe_4S_4 clusters as small molecule catalysts. *Nature Catalysis* **2018**, *1*, 383−384.

(4) Wang, S. C.; Frey, P. A. S-adenosylmethionine as an oxidant: the radical SAM superfamily. *Trends Biochem. Sci.* **2007**, *32*, 101−110.

(5) Rettberg, L. A.; Wilcoxen, J.; Lee, C. C.; Stiebritz, M. T.; Tanifuji, K.; Britt, R. D.; Hu, Y. Probing the coordination and function of Fe_4S_4 modules in nitrogenase assembly protein NifB. *Nat. Commun.* **2018**, *9*, 2824.

(6) Mouesca, J.-M.; Lamotte, B. Iron−sulfur clusters and their electronic and magnetic properties. *Coord. Chem. Rev.* **1998**, *178*−*180*, 1573−1614.

(7) Read, A. D.; Bentley, R. E.; Archer, S. L.; Dunham-Snary, K. J. Mitochondrial iron-sulfur clusters: Structure, function, and an emerging role in vascular biology. *Redox Biology* **2021**, *47*, 102164.

(8) Zanello, P. The competition between chemistry and biology in assembling iron−sulfur derivatives. Molecular structures and electrochemistry. Part V. $\{[Fe_4S_4](SCys\gamma)_4\}$ proteins. *Coord. Chem. Rev.* **2017**, *335*, 172−227.

(9) Torres, R. A.; Lovell, T.; Noodleman, L.; Case, D. A. Density functional and reduction potential calculations of Fe_4S_4 clusters. *J. Am. Chem. Soc.* **2003**, *125*, 1923−1936.

(10) Lo, W.; Scott, T. A.; Zhang, P.; Ling, C.-C.; Holm, R. H. Stabilities of cubane type $[Fe_4S_4(SR)_4]^{2-}$ clusters in partially aqueous media. *Journal of Inorganic Biochemistry* **2011**, *105*, 497−508.

(11) Waser, V.; Ward, T. R. Aqueous stability and redox chemistry of synthetic $[Fe_4S_4]$ clusters. *Coord. Chem. Rev.* **2023**, *495*, 215377.

(12) Backes, G.; Mino, Y.; Loehr, T. M.; Meyer, T. E.; Cusanovich, M. A.; Sweeney, W. V.; Adman, E. T.; Sanders-Loehr, J. The environment of Fe_4S_4 clusters in ferredoxins and high-potential iron proteins. New information from x-ray crystallography and resonance Raman spectroscopy. *J. Am. Chem. Soc.* **1991**, *113*, 2055−2064.

(13) Liu, J.; Chakraborty, S.; Hosseinzadeh, P.; Yu, Y.; Tian, S.; Petrik, I.; Bhagi, A.; Lu, Y. Metalloproteins Containing Cytochrome, Iron−Sulfur, or Copper Redox Centers. *Chem. Rev.* **2014**, *114*, 4366−4469.

(14) Sharp, C. R.; Duncan, J. S.; Lee, S. C. $[Fe_4S_4]^q$ Cubane Clusters (q = 4+, 3+, 2+) with Terminal Amide Ligands. *Inorg. Chem.* **2010**, *49*, 6697−6705.

(15) Kyritsis, P.; Hatzfeld, O. M.; Link, T. A.; Moulis, J.-M. The Two [4Fe-4S] Clusters in Chromatium vinosumFerredoxin Have Largely Different Reduction Potentials: STRUCTURAL ORIGIN AND FUNCTIONAL CONSEQUENCES. *J. Biol. Chem.* **1998**, *273*, 15404−15411.

(16) Sharma, A. K.; Kim, N.; Cameron, C. S.; Lyndon, M.; Gorman, C. B. Dendritically Encapsulated, Water-Soluble Fe_4S_4: Synthesis and Electrochemical Properties. *Inorg. Chem.* **2010**, *49*, 5072−5078.

(17) Hill, C. L.; Renaud, J.; Holm, R. H.; Mortenson, L. E. Synthetic analogs of the active sites of iron-sulfur proteins. 15. Comparative polarographic potentials of the $[Fe_4S_4(SR)_4]^{2-,3-}$ and Clostridium pasteurianum ferredoxin redox couples. *J. Am. Chem. Soc.* **1977**, *99*, 2549−2557.

(18) Ueyama, N.; Yamada, Y.; Okamura, T. A.; Kimura, S.; Nakamura, A. Structure and Properties of $[Fe_4S_4\{2,6\text{-bis(acylamino)benzenethiolato-S}\}_4]^{2-}$ and $[Fe_2S_2\{2,6\text{-bis(acylamino)benzenethiolato-S}\}_4]^{2-}$: Protection of the Fe-S Bond by Double NH···S Hydrogen Bonds. *Inorg. Chem.* **1996**, *35*, 6473−6484.

(19) Berg, J. M.; Hodgson, K. O.; Holm, R. H. Crystal structure of $[(C_2H_5)_4N]_3[Fe_4S_4(SCH_2Ph)_4]$, a reduced ferredoxin site analog with a nontetragonal Fe_4S_4 core structure in the solid state. *J. Am. Chem. Soc.* **1979**, *101*, 4586−4593.

(20) Dey, A.; Jenney, F. E.; Adams, M. W. W.; Babini, E.; Takahashi, Y.; Fukuyama, K.; Hodgson, K. O.; Hedman, B.; Solomon, E. I. Solvent Tuning of Electrochemical Potentials in the Active Sites of HiPIP Versus Ferredoxin. *Science* **2007**, *318*, 1464−1468.
(21) Gaughan, S. J. H.; Hirst, J. D.; Croft, A. K.; Jäger, C. M. Effect of Oriented Electric Fields on Biologically Relevant Iron−Sulfur Clusters: Tuning Redox Reactivity for Catalysis. *J. Chem. Inf. Model.* **2022**, *62*, 591−601.
(22) Ali, F. A.; Shafaa, M. W.; Amin, M. A. Computational Approach for Probing Redox Potential for Iron-Sulfur Clusters in Photosystem I. *Biology* **2022**, *11*, 362.
(23) Era, I.; Kitagawa, Y. A.-O.; Yasuda, N.; Kamimura, T.; Amamizu, N.; Sato, H.; Cho, K.; Okumura, M.; Nakano, M. A.-O. Theoretical Study on Redox Potential Control of Iron-Sulfur Cluster by Hydrogen Bonds: A Possibility of Redox Potential Programming. *Molecules* **2021**, *26*, 6129.
(24) Jafari, S.; Tavares Santos, Y. A.; Bergmann, J.; Irani, M.; Ryde, U. Benchmark Study of Redox Potential Calculations for Iron−Sulfur Clusters in Proteins. *Inorg. Chem.* **2022**, *61*, 5991−6007.
(25) Noodleman, L.; Lovell, T.; Liu, T.; Himo, F.; Torres, R. A Insights into properties and energetics of iron-sulfur proteins from simple clusters to nitrogenase. *Curr. Opin. Chem. Biol.* **2002**, *6*, 259−273.
(26) Sharma, S.; Sivalingam, K.; Neese, F.; Chan, G. K.-L. Low-energy spectrum of iron−sulfur clusters directly from many-particle quantum mechanics. *Nat. Chem.* **2014**, *6*, 927−933.
(27) Xiao, Y.; Koutmos, M.; Case, D. A.; Coucouvanis, D.; Wang, H.; Cramer, S. P. Dynamics of an $[Fe_4S_4(SPh)_4]^{2-}$ cluster explored via IR, Raman, and nuclear resonance vibrational spectroscopy (NRVS)-analysis using ^{36}S substitution, DFT calculations, and empirical force fields. *Dalton Transactions* **2006**, *10*, 2192−2201.
(28) Dey, A.; Roche, C. L.; Walters, M. A.; Hodgson, K. O.; Hedman, B.; Solomon, E. I. Sulfur K-Edge XAS and DFT Calculations on $[Fe_4S_4]^{2+}$ Clusters: Effects of H-bonding and Structural Distortion on Covalency and Spin Topology. *Inorg. Chem.* **2005**, *44*, 8349−8354.
(29) Bergeler, M.; Stiebritz, M. T.; Reiher, M. Structure−Property Relationships of Fe_4S_4 Clusters. *ChemPlusChem.* **2013**, *78*, 1082−1098.
(30) Czernuszewicz, R. S.; Macor, K. A.; Johnson, M. K.; Gewirth, A.; Spiro, T. G. Vibrational mode structure and symmetry in proteins and analogs containing Fe_4S_4 clusters: resonance Raman evidence that HiPIP is tetrahedral while ferredoxin undergoes a D_{2d} distortion. *J. Am. Chem. Soc.* **1987**, *109*, 7178−7187.
(31) Averill, B. A.; Herskovitz, T.; Holm, R. H.; Ibers, J. A. Synthetic analogs of the active sites of iron-sulfur proteins. II. Synthesis and structure of the tetra[mercapto- μ_3-sulfido-iron] clusters, $[Fe_4S_4(SR)_4]^2$. *J. Am. Chem. Soc.* **1973**, *95*, 3523−3534.
(32) Niu, S.; Ichiye, T. Insight into Environmental Effects on Bonding and Redox Properties of [4Fe-4S] Clusters in Proteins. *J. Am. Chem. Soc.* **2009**, *131*, 5724−5725.
(33) Niu, S.; Ichiye, T. Probing the structural effects on the intrinsic electronic and redox properties of $[2Fe−2S]^+$ clusters, a broken-symmetry density functional theory study. *Theor. Chem. Acc.* **2007**, *117*, 275−281.
(34) Wang, X.-B.; Niu, S.; Yang, X.; Ibrahim, S. K.; Pickett, C. J.; Ichiye, T.; Wang, L.-S. Probing the Intrinsic Electronic Structure of the Cubane [4Fe−4S] Cluster: Nature's Favorite Cluster for Electron Transfer and Storage. *J. Am. Chem. Soc.* **2003**, *125*, 14072−14081.

https://doi.org/10.1021/acs.jpclett.5c00616
J. Phys. Chem. Lett. 2025, 16, 4602−4606